HOKKAIDO UNIVERSITY

Title	Formation and field-assisted dissolution of anodic films on iron in fluoride-containing organic electrolyte
Author(s)	Shahzad, Khurram; Tsuji, Etsushi; Aoki, Yoshitaka et al.
Citation	Electrochimica acta, 151, 363-369 https://doi.org/10.1016/j.electacta.2014.10.132
Issue Date	2015-01-01
Doc URL	https://hdl.handle.net/2115/57952
Type	journal article
File Information	E_field_EA_rev.pdf

Hokkaido University Collection of Scholarly and Academic Papers : HUSCAP

Formation and field-assisted dissolution of anodic films on iron in fluoride-containing organic electrolyte

Khurram Shahzad[a], Etsushi Tsuji[a,b], Yoshitaka Aoki[a,b], Shinji Nagata[c], and Hiroki Habazaki[a,b,1,*]

[a] Graduate School of Chemical Sciences and Engineering, Hokkaido University, Sapporo, Hokkaido 060-8628, Japan

[b] Division of Materials Chemistry & Frontier Chemistry Center, Faculty of Engineering, Hokkaido University, Sapporo, Hokkaido 060-8628, Japan

[c] Institute for Materials Research, Tohoku University, 2-1-1, Katahira, Aoba-ku, Sendai 980-8577, Japan

*Corresponding author: habazaki@eng.hokudai.ac.jp, TEL & FAX: +81-11-706-6575

[1] ISE member

Abstract:

Magnetron-sputtered iron films were potentiodynamically anodized at two different sweep rates to 50 V in an ethylene glycol electrolyte containing ammonium fluoride and water. At a high sweep rate of 1.0 V s^{-1}, a barrier-type anodic film was formed even though the current efficiency was as low as ~50%. In contrast, a nanoporous anodic film developed at a low sweep rate of 0.05 V s^{-1}, and the film-formation efficiency reduced to 37%. The main part of the anodic films consists of iron (III) hydroxyfluoride with a thin inner layer composed of FeF_3. The inner fluoride layer is formed owing to the faster inward migration of fluoride ions compared to that of the oxygen species. During immersion or re-anodizing of the iron specimen with an approximately 100-nm-thick, barrier-type anodic film at and below 15 V, thinning of the anodic film proceeded uniformly and film dissolution was enhanced by applying an electric field. The impact of the electric field on film formation and dissolution is discussed.

Keywords: Anodizing, iron, porous anodic film, organic electrolyte, fluoride

1. Introduction

Nanoporous oxide films, formed by anodizing valve metals such as Al, Ti, Zr, Nb, Ta, and W, have been extensively explored in the last two decades because of their practical importance as well as of fundamental interest in the growth mechanism. These films have potential applications in corrosion protection, nanodevices, solar cells, batteries, and templates for the fabrication of various nanomaterials [1-4]. There are three types of anodic films: barrier-type, nanoporous-type, and nanotubular-type. Their formation depends upon the anodizing conditions, such as the anodizing electrolyte and anodizing voltage/current. The barrier-type anodic films are typically formed when growth proceeds at a high current efficiency. When the films are amorphous, new film materials are developed both at the film/electrolyte and metal/film interfaces by outward migration of cations and inward migration of anions, respectively, in a corporative manner [5].

The formation behavior of self-organized porous oxide films has attracted much attention in recent years. It is well accepted that porous anodic films are formed when new film material is formed only at the metal/film interface, while cation species migrating outwards are ejected directly to the electrolyte at the film/electrolyte interface [6]. Most recent studies have focused on the understanding of the mechanism of pore generation, and efforts have been made to resolve the causes of field-induced and stress-induced instabilities at the

52 film/electrolyte interface, which leads to pore formation [7-10]. It is generally presumed that
53 pores initiate at a rough film/electrolyte interface under an electric field, where the field is
54 non-uniformly concentrated at the troughs of the film/electrolyte interface. Various
55 mechanisms have been proposed for the growth of porous oxides over the past 50 years,
56 namely (a) field-induced dissolution, (b) field-assisted ejection, and (c) field-assisted plastic
57 flow [6, 8, 11, 12]. In the field assisted dissolution model, first proposed by Hoar and Mott
58 [13], it is presumed that the generation of pores is associated with the dynamic equilibrium
59 between the rate of oxide formation at the metal/film interface and the dissolution of the oxide
60 at the film/electrolyte interface. Most investigations in the field-assisted dissolution model
61 assume that steady-state film growth kinetics occur due to an accelerating dissolution of the
62 oxide film under the influence of a high external electric field at the pore base [6, 11, 13, 14].

63 Recently, Garcia et al. proposed that the generation and growth of a porous anodic
64 structure on aluminum is associated with the field-assisted flow of oxide material by a
65 distribution of compressive stresses [12, 15-18]. Through a series of tracer experiments, they
66 concluded that pores are generated by plastic flow of material from the pore base towards the
67 cell walls in certain electrolytes. In parallel, Hebert and co-workers support their flow model
68 using a computational approach [8, 19].

In both field-assisted dissolution and field-assisted flow models, the electric field applied in the barrier layer sandwiched between the porous layer and metal substrate plays a crucial role. Direct experimental evidences of the influence of the electric field on dissolution and pore initiation and the presence of a critical field for pore initiation during the anodizing of aluminum have been demonstrated recently by Oh and Thomson [9]. They showed that uniform thinning of the oxide film occurs below a field of 7.46 MV cm^{-1}, and field-induced instability and pore initiation start at this critical field. The mechanical instability that leads to major pore formation begins at 8.9 MV cm^{-1}.

As mentioned above, porous anodic films can be formed on a range of metals. Fluoride-containing organic electrolytes with a small amount of water have been often used for the formation of porous anodic films on titanium [20], zirconium [21], niobium [22], and iron [23-27]. The nanoporous and nanotubular anodic films formed on iron have attracted attention due to their future promising applications, including photoanodes for water splitting, electrodes for lithium ion batteries, gas sensors, and electrodes for electrochemical capacitors [27-32]. Photoelectrochemical characterization of as-anodized and thermally treated anodicfilmson iron was also carried out in details [33]. Despite extensive investigations on the mechanism of porous film formation on aluminum, studies on the formation mechanism of porous anodic films on iron have been very limited [23-25].

In the present study, we first formed barrier-type and nanoporous-type anodic films on iron by potentiodynamic anodizing in an ethylene glycol electrolyte containing ammonium fluoride and water, and their formation behavior was examined. Then, the influence of an electric field on dissolution rate of anodic films on iron was investigated by applying an electric field to the pre-formed barrier-type anodic film in order to elucidate the crucial role of the electric field in anodizing iron.

2. Experimental

Iron thin films of ~ 460 nm thickness were prepared by DC magnetron sputtering. The target was a 99.9% pure iron disk of 0.5 mm thickness and 100 mm diameter bonded on a copper backing plate. Glass plates and electropolished, anodized aluminum sheets were used as the substrate. The latter substrates were used for Rutherford backscattering spectroscopy (RBS) analysis.

The iron thin films were potentiodynamically anodized at varying sweep rates (1.0 and 0.05 V s^{-1}) in a two-electrode cell with a platinum sheet as the counter electrode. The electrolyte was ethylene glycol (EG) containing 0.1 mol L^{-1} ammonium fluoride and 0.1 mol L^{-1} water at 273 K. After anodizing, the specimens were washed in EG and then in acetone. The relatively low temperature and low water concentration in the electrolyte was selected to

105 reduce the chemical dissolution rate and to promote the formation of a barrier –type film to
106 higher formation voltages.

107 The surfaces and cross-sections of the anodized iron specimens were observed using
108 a JEOL JSM-6500F field emission scanning electron microscope operated at an accelerating
109 voltage of 10 kV. The composition of the anodic films were determined by RBS using a He^{2+}
110 ion beam of 2.0 MeV energy supplied by a tandem-type accelerator at Tohoku University.
111 The RBS data were analyzed using the RUMP program [34].
112

113 **3. Results and Discussion**

114 3.1. Potentiodynamic growth of anodic films

115 Magnetron-sputtered iron films were potentiodynamically anodized to 50 V at 1.0
116 and 0.05 V s^{-1} in the EG electrolyte containing 0.1 mol L^{-1} NH_4F and 0.1 mol L^{-1} H_2O at 273
117 K. The typical current-voltage responses are shown in Fig. 1. Initially, the current density
118 increases almost linearly to a current peak, followed by a current decrease to a steady-state
119 current density. At the potential sweep rate of 0.05 V s^{-1}, a second small current peak appears
120 at 12 V, in addition to the first higher current peak at 4 V. Assuming that uniform thickening
121 of the anodic film occurs, the growth of the barrier anodic film can be described by the
122 following equation,

$$\frac{dV}{dt} = E\frac{dh}{dt} \quad (1)$$

where V is the applied voltage, t is the anodizing time, E is the electric field across the anodic film, and h is the thickness of the anodic film. Considering Faraday's law, the following equation can be described,

$$\frac{dV}{dt} = \frac{\eta EMi}{zF} \quad (2)$$

where η is the current efficiency for film growth, M is the molar volume, i is the anodizing current, z is the equivalent number, and F is Faraday's constant. This equation suggests that under a constant potential sweep rate (dV/dt = constant), current becomes constant under a steady state condition, as in the case of Fig. 1. The presence of the current peak at a low voltage region during potentiodynamic anodizing has been found often in the anodizing of valve metals. The phenomenon was well discussed in a review paper by Lorengel [35] and explained in terms of a delayed oxide formation.

Although there are only limited studies on anodic film growth under potentiodynamic conditions [36-38], Curioni et al. potentiodynamically anodized high purity aluminum in a sulfuric acid electrolyte [36]. In contrast to the observation of a steady-state current in the present study, they found a continuous current increase above a narrow plateau potential region less than 3 V. This was interpreted by the flow model, which was valid in anodizing aluminum in sulfuric acid [7, 39]. Because of the flow of film material, part of the

anodic oxide generated at the metal/film interface is displaced to the cell walls. The displacement tends to reduce the thickness of the barrier layer, contributing to an increase in the electric field and current density. Even though a porous film is formed at the low potential sweep rate as indicated below, the absence of such a continuous current increase in the present study may suggest that the flow model is not applicable here.

Fig. 2 shows the scanning electron micrographs of surfaces of the magnetron-sputtered iron films as-deposited and anodized to 50 V at 0.05 and 1.0 V s^{-1}. Associated with the columnar structure of the as-deposited film, a relatively rough surface is observed in Fig. 2a. The apparent grain size (column width) is 50–100 nm. Similar surface morphology is observed after anodizing to 50 V at 1.0 V s^{-1} (Fig. 2b), with troughs along the grain boundaries; however, the surface appears to be smoother within grains. For the iron film anodized at the low sweep rate (Fig. 2c), nanopores develop with an average pore size of ~10 nm. The nanopores are formed preferentially at the trough region of the rough surface. Similar results were reported previously in the anodizing of carbon steel [40] as well as aluminum [2]. This means that the site of pore initiation can be controlled by texturing of the metal surface prior to anodizing of iron.

The formation of a barrier-type anodic film at the high sweep rate of 1.0 V s^{-1} is confirmed from the scanning electron micrograph of a cross-section of the anodized iron

159 specimen (Fig. 3a). On the columnar iron layer, a compact anodic film of 100 ± 5 nm
160 thickness developed. The metal/film interface is relatively flat, while the film/electrolyte
161 interface is rough, though barrier-type films formed at high current efficiency typically have a
162 flat film/electrolyte interface. A similar rough film/electrolyte interface and/or a thin porous
163 layer above a barrier layer was found when aluminum was potentiodynamically anodized to
164 40 V in a tartaric acid electrolyte; no film material was formed at the film/electrolyte interface
165 due to direct ejection of outwardly migrating Al^{3+} ions [41]. As discussed later, no film
166 material is formed at the film/electrolyte interface because of the low current efficiency in the
167 formation of the present barrier-type anodic film on iron. In the anodic film formed at the low
168 sweep rate, cylindrical nanopore channels are developed (Fig. 3b). The thickness of the
169 anodic film is 400 ± 7 nm and the barrier layer, sandwiched between the porous layer and iron
170 substrate, has a thickness of 72 ± 5 nm, which is slightly thinner than that formed at the high
171 sweep rate. The interpore distance is ~ 60 nm. When anodizing aluminum in acid electrolytes,
172 the interpore distance is controlled by the formation voltage (2.5–2.8 nm V^{-1}) [14]. Since the
173 thickness of the barrier layer beneath the porous alumina layer is ~1.0 nm V^{-1}, the interpore
174 distance of the porous layer for porous anodic alumina is 2.5–2.8 times the thickness of the
175 barrier layer. Compared with the morphology of the porous alumina films, the interpore
176 distance in the porous film on iron is too small with respect to the thickness of the barrier
177 layer. The interpore distance of the anodic film on iron appears to be similar to the column

178 width of the deposited iron. Considering the preferential formation of pores at the trough
179 region of the as-deposited iron surface, it is likely that the interpore distance is controlled by
180 the morphology of the iron surface, not the anodizing parameters under the present anodizing
181 condition. Field-assisted dissolution, rather than field-assisted flow, appears to be dominant in
182 growing porous films on iron under the present conditions.

183 The composition of the anodic films formed on iron was examined by RBS. Fig. 4
184 shows the experimental and simulated RBS spectra of the as-deposited iron films and
185 anodized to 50 V at the sweep rates of 1.0 and 0.05 V s^{-1}. The RBS spectrum of the
186 as-deposited iron (Fig. 4a) shows yields from iron, aluminum, and oxygen, with the latter two
187 arising from the anodized aluminum substrate. In Fig. 4b, yields from fluorine and oxygen in
188 the anodic film appear separately from the other yields, and a higher yield of fluorine in
189 comparison with oxygen indicates that the anodic film is fluoride-rich. In Fig. 4c, the yield
190 from oxygen appears again, but the yield from fluorine is overlapped with that from iron. The
191 precise composition of the anodic films was examined by simulation. The simulated spectra,
192 shown in Figs. 4b and 4c, obtained using the composition, density, and thicknesses of
193 individual layers in Table 1, are fit with the respective experimental spectra. In the simulation,
194 probable incorporation of carbon species derived from EG into the anodic films was neglected
195 due to a low RBS sensitivity for carbon. The anodic film formed at the high sweep rate

196 consists of two layers: the outer layer (composed of iron (III) hydroxyfluoride or hydrated
197 oxyfluoride) and the inner layer (composed of iron (III) fluoride). The formation of the inner
198 fluoride layer may be associated with the faster inward migration of fluoride ions compared
199 with oxygen species, as reported previously [25]. The faster migration of fluoride in growing
200 barrier-type anodic films has also been reported in the anodizing of tantalum [42] and
201 titanium [43]. The outer layer of the present barrier-type anodic film is composed of hydrated
202 oxide or contains hydroxide. Since the anodic film formed under the present condition is
203 soluble in water, there is a possibility that the hydration proceeded in laboratory air after
204 anodizing, not during anodizing.

205 The porous anodic film formed at the low sweep rate also has a compositionally
206 layered structure. The porous layer, 328 nm thick, is composed of hydrated hydroxyfluoride
207 and a barrier layer of 72 nm thickness. Both layers have a composition similar to the
208 respective layers formed at the high sweep rate.

209 From the comparison, determined by the RBS spectra of as-deposited iron films
210 anodized to 50 V, the thicknesses consumed by anodizing were 40 ± 3 and 75 ± 3 nm at the
211 high and low sweep rates, respectively. Assuming that iron was oxidized to the Fe (III) state,
212 the respective electric charges required to oxidize iron were 0.16 ± 0.02 and 0.31 ± 0.02 C
213 cm^{-2}, as shown in Table 2. The electric charges passed during anodizing to 50 V at the high

214 and low sweep rates were 0.15 ± 0.01 and 0.57 ± 0.02 C cm^{-2}, respectively. It is obvious from
215 these results that the electric charge passed during anodizing is used predominantly for the
216 oxidation of iron at the high sweep rate, while it reduces to 54% at the low sweep rate. During
217 anodizing at the low sweep rate, gas generation was observed, to a minor extent, from the
218 specimen surface, contributing to the reduction of the efficiency of iron oxidation. The likely
219 presence of gas bubbles in the barrier layer may also contribute to the reduction of the barrier
220 layer thickness (~72 nm) in comparison with that at the high sweep rate. The electric charge
221 used for the formation of anodic films was also calculated from the number of iron (III) ions
222 in the anodic films and the current efficiency for film formation was then estimated (Table 2).
223 Although a barrier-type film is formed at the high sweep rate, the current efficiency is only
224 49%. It is likely that film materials are formed only at the metal/film interface by inward
225 migration of anions and the direct ejection of outwardly migrating cation species occurs at the
226 film/electrolyte interface; the latter contributes to the reduced efficiency of film formation. At
227 the low sweep rate, the current efficiency is further reduced to 37%, but 68% of the oxidized
228 iron was converted to the anodic film. The increased conversion efficiency during porous film
229 growth at the low sweep rate, compared with that for the barrier film growth at the high sweep
230 rate, is of interest, being related to the field-assisted dissolution process and/or the probable
231 presence of oxygen gas bubbles in the barrier layer formed at the low sweep rate. Thus, the
232 field-assisted dissolution was examined in detail.

233

234 3.2. Field-assisted dissolution

235 In order to examine the influence of an electric field on the dissolution of anodic
236 films formed on iron, a barrier-type film of 100 nm thickness was first formed by anodizing
237 the magnetron-sputtered iron film to 50 V at the high sweep rate of 1.0 V s^{-1}. Then, several
238 constant voltages were applied to the anodized specimen and the change in the film thickness
239 was examined. Fig. 5 shows the change in the current density during the re-anodizing of the
240 iron/anodic film (100 nm) specimen, at 10, 15, 20, and 30 V. The current density is initially
241 very low at 10 V, since the pre-formed anodic film was developed to 50 V and the initial field
242 strength is too low for ion migration. However, the current density gradually increases with
243 time. The initial, very low, current is also found at 15 V, but the current increase occurs from
244 the commencement of re-anodizing when 20 and 30V is applied.

245 Fig. 6 shows scanning electron micrographs of cross-sections before and after
246 re-anodizing at several voltages for 1000 s. It is obvious that the anodic film of approximately
247 100 nm thickness (Fig. 6a) shows a uniform thickness reduction to 76 nm after re-anodizing at
248 10 V for 1000 s (Fig. 6b). A further reduced thickness to 67 nm is observed at 15 V (Fig. 6c),
249 indicating that an electric field-assisted dissolution occurs. During re-anodizing at these
250 voltages, the morphology of the anodic films does not change; no porous film is developed. In

contrast, thickening of the anodic film takes place at 20 V (Fig. 6d). Although the pores are not clearly seen in the anodic film at the available SEM resolution, a porous film must be grown for film thickening at 20 V. Thickening of the porous film was clearly observed after re-anodizing at 30 V (Fig. 6e).

The change in the anodic film thickness during immersion and re-anodizing at 10 and 15 V (Fig. 7a) shows an accelerated dissolution under an applied electric field. During immersion of the pre-anodized specimen, film thinning occurs at a rate of 0.47 nm min^{-1}. The dissolution rate is enhanced by applying 10 and 15 V, with the latter voltage resulting in a more enhanced dissolution rate. Since the thickness reduction occurs during re-anodizing, the electric field across the barrier layer changes. The change in the electric field with re-anodizing time is shown in Fig. 7b. Since the field-assisted dissolution is found at 10 V and a re-anodizing time of 600 s, an electric field of 1.2 MV cm^{-1} appears to be sufficient to enhance the dissolution of the anodic film on iron. This electric field is much lower than that for anodic alumina (5.5 MV cm^{-1}), as examined by Oh and Thompson [9]. Oh and Thompson also reported the presence of a critical field (7.46 MV cm^{-1}) for pore initiation due to field-induced instability. In the anodic film on iron, the critical field must be higher than 2.8 MV cm^{-1}, since no pores were found when the electric field was increased to this value at 15 V (Fig. 7b).

In summary, anodizing iron in a fluoride-containing EG electrolyte, the electric field has a crucial role in the dissolution and morphology of the anodic films, as with aluminum in acid electrolytes. Major pores formed by the mechanical instability (flow of film materials), found in the anodizing of aluminum, were not formed under the present anodizing condition for iron. Thus, pores formed due to field-assisted dissolution appear to be dominant in the anodizing of iron.

4. Conclusions

Anodic films are formed on magnetron-sputtered iron films by potentiodynamic anodizing to 50 V at two different sweep rates of 1.0 and 0.05 V s^{-1} in an EG electrolyte containing 0.1 mol L^{-1} NH_4F and 0.1 mol L^{-1} H_2O at 273K. The film morphology is dependent upon the sweep rate: a barrier-type at the high sweep rate and a nanoporous-type at the low sweep rate. The barrier-type film is formed even at a low current efficiency of 49%, suggesting no film material develops at the film/electrolyte interface. In contrast, a nanoporous anodic film develops by anodizing to the same 50 V at the low sweep rate of 0.05 V s^{-1}. Pores are developed preferentially along with the surface troughs, which corresponds to the boundaries of the columnar morphology. The anodic films compositionally consist of an outer iron (III)

hydroxyfluoride layer and an inner FeF_3 layer; the latter layer forming because of the faster migration of fluoride ions in comparison with that of the oxygen species.

When an electric field is applied to the barrier-type anodic film formed by sweeping to 50 V at the high sweep rate, chemical dissolution at the film/electrolyte interface is accelerated. The field-assisted dissolution is also of importance in anodizing iron to form nanoporous anodic films. No evidence of plastic flow from the pore base to the cell walls is found under the present anodizing conditions.

Acknowledgments

This work was supported in part by the "Nanotechnology Platform" program of the Ministry of Education, Culture, Sports, Science and Technology (MEXT), Japan.

References

[1] C. Blawert, W. Dietzel, E. Ghali, G.L. Song, Adv. Eng. Mater., 8 (2006) 511-533.

[2] H. Masuda, K. Fukuda, Science, 268 (1995) 1466-1468.

[3] T. Kyotani, L.-f. Tsai, A. Tomita, Chem. Mater., 7 (1995) 1427-1428.

[4] P. Roy, S. Berger, P. Schmuki, Angew. Chem., Int. Ed., 50 (2011) 2904-2939.

[5] L. Young, D.J. Smith, J. Electrochem.Soc., 126 (1979) 765-768.

304 [6] G.E. Thompson, Thin Solid Films, 297 (1997) 192-201.

305 [7] S.J. Garcia-Vergara, L. Iglesias-Rubianes, C.E. Blanco-Pinzon, P. Skeldon, G.E.

306 Thompson, P. Campestrini, Proceedings of the Royal Society A: Mathematical, Physical

307 and Engineering Sciences, 462 (2006) 2345-2358.

308 [8] J.E. Houser, K.R. Hebert, Nat. Mater., 8 (2009) 415-420.

309 [9] J. Oh, C.V. Thompson, Electrochim. Acta, 56 (2011) 4044-4051.

310 [10] K.R. Hebert, S.P. Albu, I. Paramasivam, P. Schmuki, Nat. Mater., 11 (2012) 162-166.

311 [11] G.E. Thompson, R.C. Furneaux, G.C. Wood, J.A. Richardson, J.S. Goode, Nature, 272

312 (1978) 433-435.

313 [12] S.J. Garcia-Vergara, P. Skeldon, G.E. Thompson, H. Habazaki, Electrochim. Acta, 52

314 (2006) 681-687.

315 [13] T.P. Hoar, N.F. Mott, J. Phys. Chem. Solids, 9 (1959) 97-99.

316 [14] J.P. O'Sullivan, G.C. Wood, Proc. R. Soc. London, A, 317 (1970) 511-543.

317 [15] F. Zhou, A. Baron-Wiecheć, S.J. Garcia-Vergara, M. Curioni, H. Habazaki, P.

318 Skeldon, G.E. Thompson, Electrochim. Acta, 59 (2012) 186-195.

319 [16] F. Zhou, A.K.M. Al-Zenati, A. Baron-Wiechec, M. Curioni, S.J. Garcia-Vergara, H.

320 Habazaki, P. Skeldon, G.E. Thompson, J. Electrochem. Soc., 158 (2011) C202-C214.

321 [17] S.J. Garcia-Vergara, D. Le Clere, T. Hashimoto, H. Habazaki, R. Skeldon, G.E.

322 Thompson, Electrochim. Acta, 54 (2009) 6403-6411.

323 [18] S.J. Garcia-Vergara, P. Skeldon, G.E. Thompson, H. Habazaki, Thin Solid Films, 515
324 (2007) 5418-5423.
325 [19] J.E. Houser, K.R. Hebert, Phys. Status Solidi A, 205 (2008) 2396-2399.
326 [20] J.M. Macak, P. Schmuki, Electrochim. Acta, 52 (2006) 1258-1264.
327 [21] S. Berger, J. Faltenbacher, S. Bauer, P. Schmuki, Physica Status Solidi-Rapid
328 Research Letters, 2 (2008) 102-104.
329 [22] W. Wei, K. Lee, S. Shaw, P. Schmuki, Chem. Commun., 48 (2012) 4244-4246.
330 [23] A. Jagminas, K. Mazeika, N. Bernotas, V. Klimas, A. Selskis, D. Baltrunas, Appl.
331 Surf. Sci., 257 (2011) 3893-3897.
332 [24] A. Jagminas, V. Klimas, K. Mazeika, N. Bernotas, A. Selskis, G. Niaura, Electrochim.
333 Acta, 56 (2011) 5452-5458.
334 [25] H. Habazaki, Y. Konno, Y. Aoki, P. Skeldon, G.E. Thompson, J. Phys. Chem. C, 114
335 (2010) 18853-18859.
336 [26] S.P. Albu, A. Ghicov, P. Schmuki, Physica Status Solidi-Rapid Research Letters, 3
337 (2009) 64-66.
338 [27] H.E. Prakasam, O.K. Varghese, M. Paulose, G.K. Mor, C.A. Grimes, Nanotechnol., 17
339 (2006) 4285-4291.
340 [28] S.K. Mohapatra, S.E. John, S. Banerjee, M. Misra, Chem. Mater., 21 (2009)
341 3048-3055.

342 [29] R.R. Rangaraju, A. Panday, K.S. Raja, M. Misra, J. Phys. D: Appl. Phys., 42 (2009)
343 135303.
344 [30] Z.H. Zhang, M.F. Hossain, T. Takahashi, Appl. Cat. B-Env., 95 (2010) 423-429.
345 [31] K.Y. Xie, J. Li, Y.Q. Lai, W. Lu, Z.A. Zhang, Y.X. Liu, L.M. Zhou, H.T. Huang,
346 Electrochem. Commun., 13 (2011) 657-660.
347 [32] H. Cheng, Z.G. Lu, R.G. Ma, Y.C. Dong, H.E. Wang, L.J. Xi, L.X. Zheng, C.K. Tsang,
348 H. Li, C.Y. Chung, J.A. Zapien, Y.Y. Li, J. Mater. Chem., 22 (2012) 22692-22698.
349 [33] M. Santamaria, S. Terracina, Y. Konno, H. Habazaki, F. Di Quarto, J. Solid State
350 Electrochem., 17 (2013) 3005-3014.
351 [34] L.R. Doolittle, Nucl. Instr. and Meth., B9 (1985) 344-351.
352 [35] M.M. Lohrengel, Mater. Sci. Eng. R-Rep., 11 (1993) 243-294.
353 [36] M. Curioni, P. Skeldon, G.E. Thompson, J. Electrochem. Soc., 156 (2009) C407.
354 [37] F. Di Franco, G. Zampardi, M. Santamaria, F. Di Quarto, H. Habazaki, J.
355 Electrochem. Soc., 159 (2012) C33-C39.
356 [38] M. Santamaria, F. Di Quarto, S. Zanna, P. Marcus, Electrochim. Acta, 56 (2011)
357 10533-10542.
358 [39] S.J. Garcia-Vergara, P. Skeldon, G.E. Thompson, H. Habakaki, Corros. Sci., 49
359 (2007) 3696-3704.

[40] Y. Konno, S. Yang, E. Tsuji, Y. Aoki, P. Skeldon, G.E. Thompson, H. Habazaki, ECS Trans., 50 (2013) 183-190.

[41] M. Curioni, T. Gionfini, A. Vicenzo, P. Skeldon, G.E. Thompson, Surf. Interface Anal., 45 (2013) 1485-1489.

[42] K. Shimizu, K. Kobayashi, G.E. Thompson, P. Skeldon, G.C. Wood, J. Electrochem. Soc., 144 (1997) 418-423.

[43] H. Habazaki, K. Fushimi, K. Shimizu, P. Skeldon, G.E. Thompson, Electrochem. Commun., 9 (2007) 1222-1227.

Figure captions

Fig. 1 *I-V* responses of magnetron-sputtered iron films at potential sweep rates of 0.05 and 1.0 V s^{-1} in an EG electrolyte containing 0.1 mol L^{-1} NH_4F and 0.1 mol L^{-1} H_2O at 273 K.

Fig. 2 Scanning electron micrographs of surfaces of the magnetron-sputtered iron films (a) as-deposited and anodized to 50 V at sweep rates of (b) 1.0 and (c) 0.05 V s^{-1} in an EG electrolyte containing 0.1 mol L^{-1} NH_4F and 0.1 mol L^{-1} H_2O at 273 K.

Fig. 3 Scanning electron micrographs of cross-sections of the magnetron-sputtered iron films anodized to 50 V at sweep rates of (a) 1.0 and (b) 0.05 V s^{-1} in an EG electrolyte containing 0.1 mol L^{-1} NH_4F and 0.1 mol L^{-1} H_2O at 273 K.

Fig. 4 Experimental and simulated RBS spectra of magnetron-sputtered iron films (a) as-deposited and anodized to 50 V at sweep rates of (b) 1.0 and (c) 0.05 V s^{-1} in an EG electrolyte containing 0.1 mol L^{-1} NH_4F and 0.1 mol L^{-1} H_2O at 273 K.

386 Fig. 5 Current transients of magnetron-sputtered iron films with a pre-formed 100-nm-thick,
387 barrier-type anodic film during re-anodizing at several constant voltages in an EG electrolyte
388 containing 0.1 mol L^{-1} NH_4F and 0.1 mol L^{-1} H_2O at 273 K.

389

390 Fig. 6 Scanning electron micrographs of cross-sections of magnetron-sputtered iron films
391 with a pre-formed 100-nm-thick, barrier-type anodic film (a) before anodizing, and after
392 re-anodizing at (b) 10 V for 1000 s, (c) 15 V for 1000 s, (d) 20 V for 1000 s, and (e) 30 V for
393 1000 s in an EG electrolyte containing 0.1 mol L^{-1} NH_4F and 0.1 mol L^{-1} H_2O at 273 K.

394

395 Fig. 7 (a) Change in thickness of the pre-formed 100-nm-thick anodic films during immersion
396 and re-anodizing at 10 and 15 V in an EG electrolyte containing 0.1 mol L^{-1} NH_4F and 0.1
397 mol L^{-1} H_2O at 273 K and (b) the respective change in the electric field associated with the
398 thinning of the anodic films.

399

400
401

402

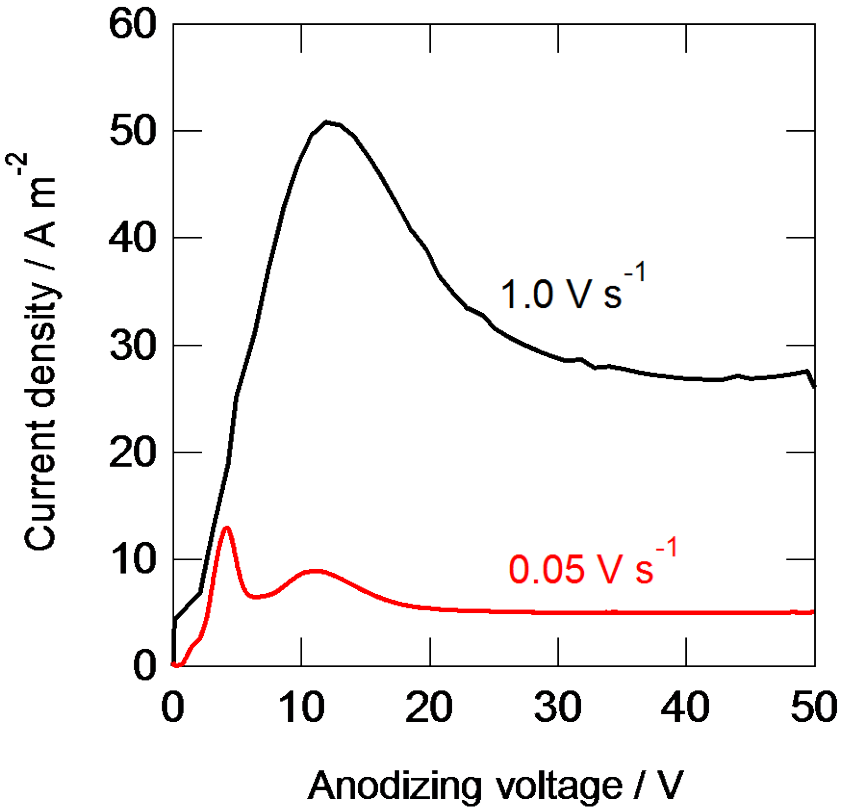
60
50
40
30
20
10
0
0
10
20
30
40
50
Current density / A m-2
Anodizing voltage / V
1.0 V s-1
0.05 V s-1

Figure 1.

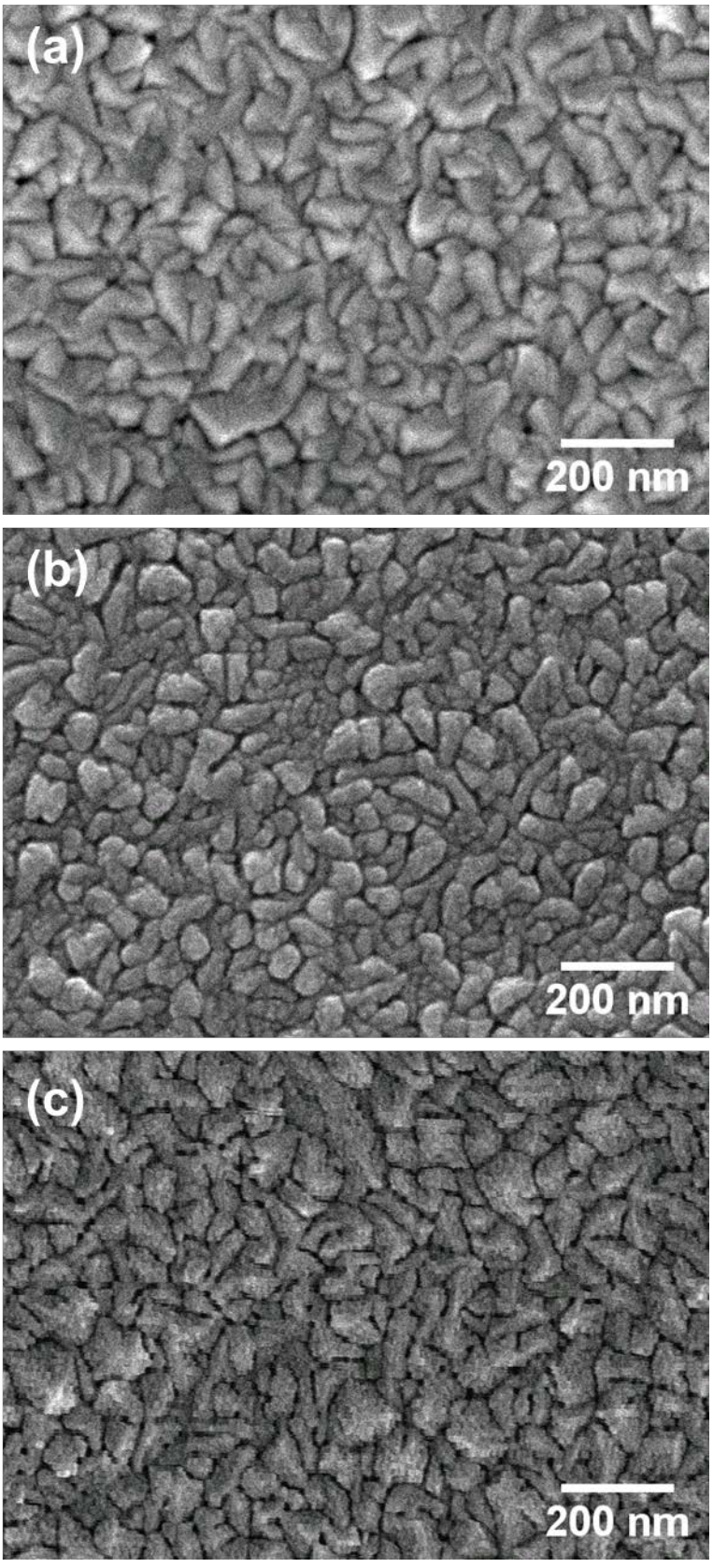

Fig. 2

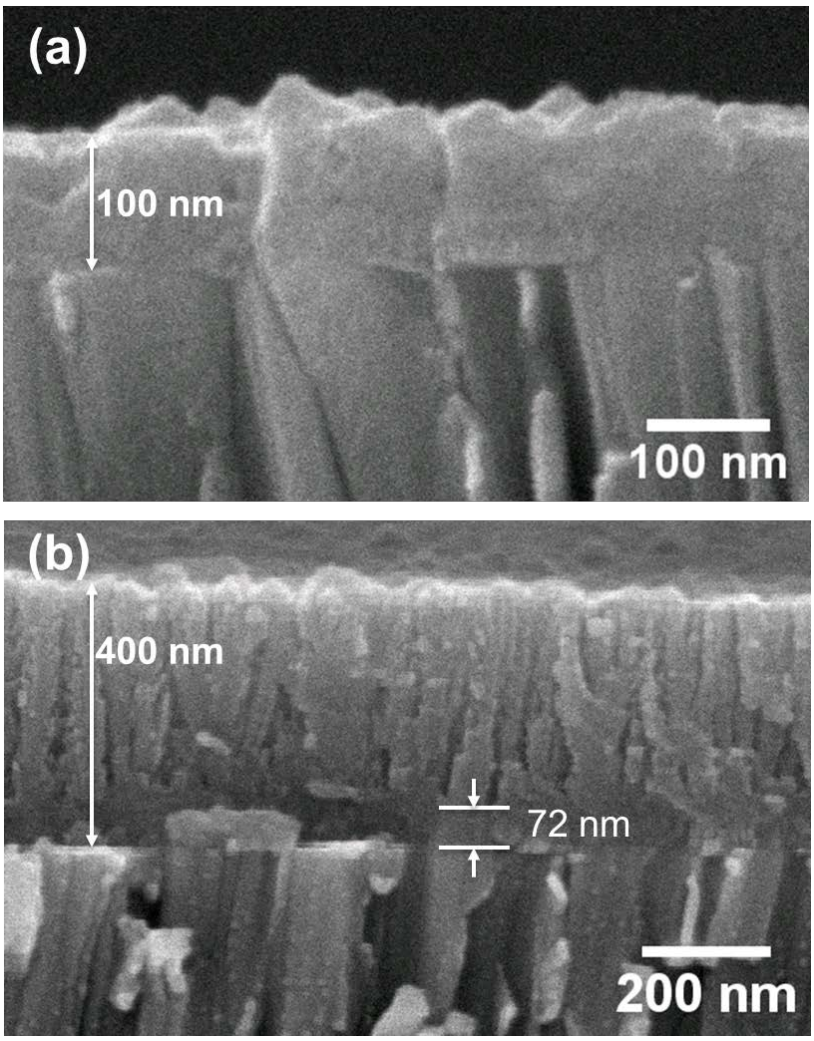

Fig. 3

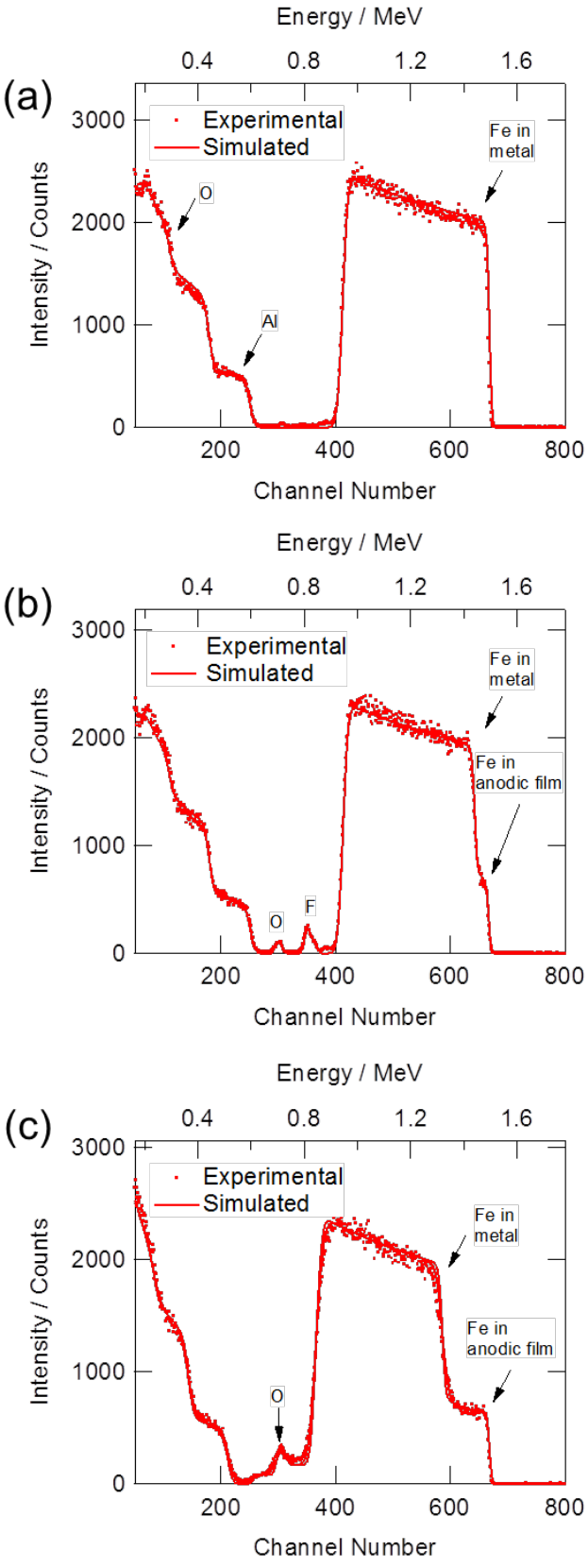
(a)
Energy / MeV
0.4
0.8
1.2
1.6
Experimental
Simulated
Fe in metal
O
Al
Intensity / Counts
3000
2000
1000
0
200
400
600
800
Channel Number
(b)
Energy / MeV
0.4
0.8
1.2
1.6
Experimental
Simulated
Fe in metal
Fe in anodic film
O
F
Intensity / Counts
3000
2000
1000
0
200
400
600
800
Channel Number
(c)
Energy / MeV
0.4
0.8
1.2
1.6
Experimental
Simulated
Fe in metal
Fe in anodic film
O
Intensity / Counts
3000
2000
1000
0
200
400
600
800
Channel Number

Fig. 4

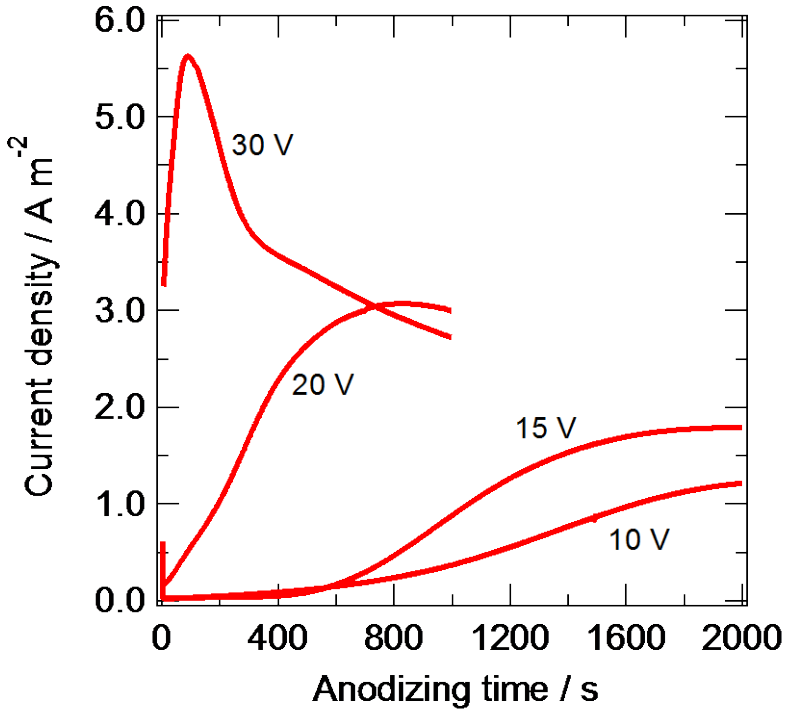
6.0
5.0
4.0
3.0
2.0
1.0
0.0
Current density / A m-2
30 V
20 V
15 V
10 V
0
400
800
1200
1600
2000
Anodizing time / s

Fig. 5

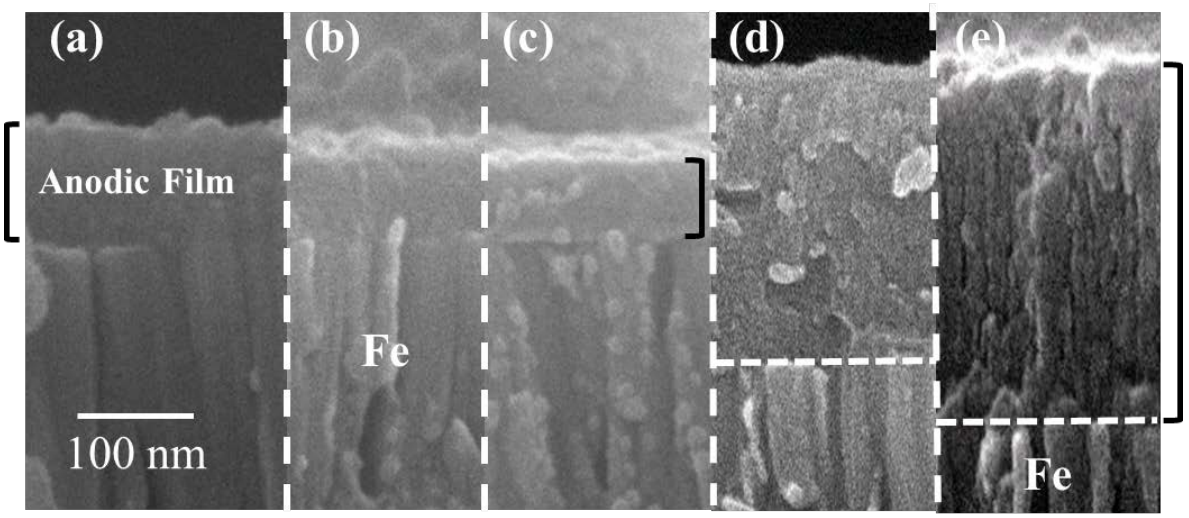

Fig. 6

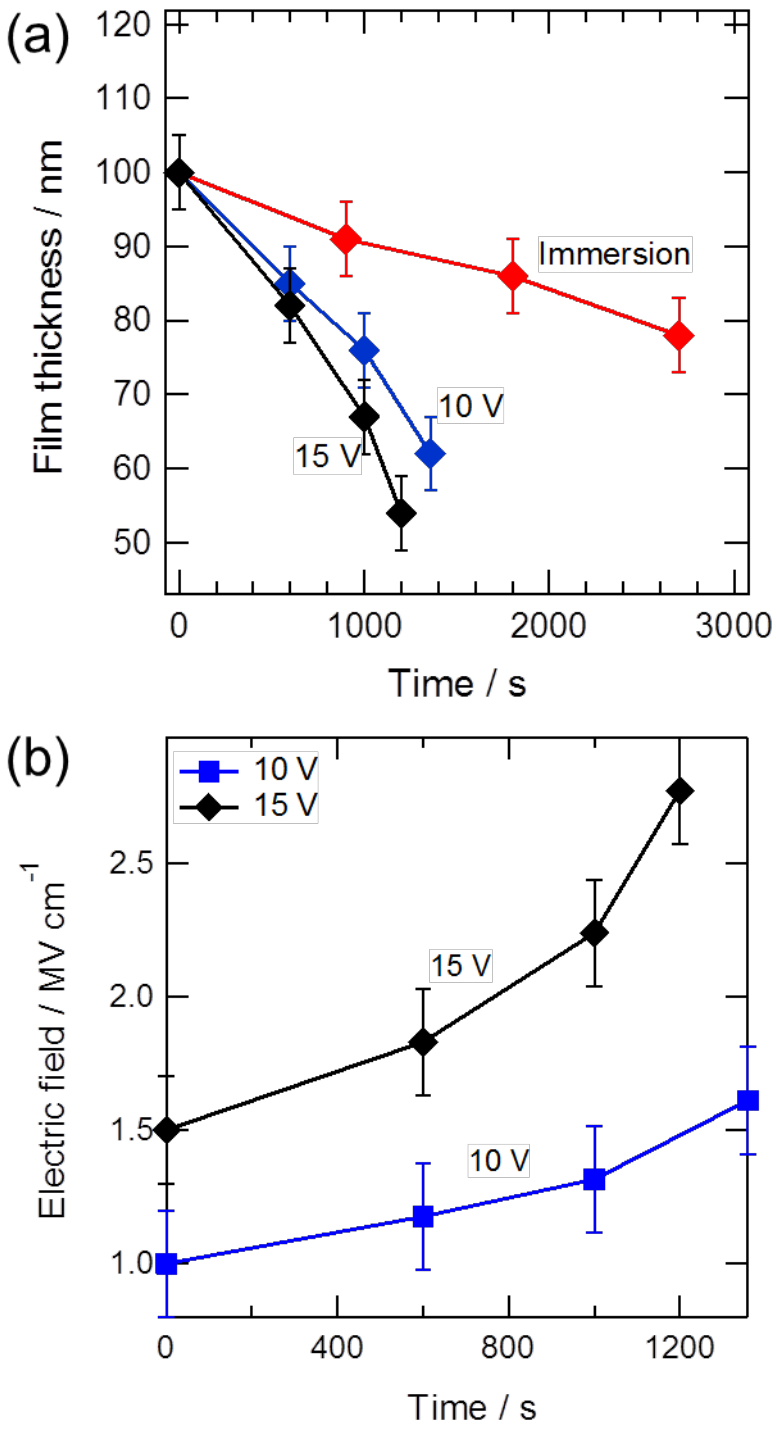
(a)
Film thickness / nm
Time / s
Immersion
10 V
15 V
(b)
Electric field / MV cm-1
Time / s
10 V
15 V

Fig. 7